The predicted properties of helium-enriched globular cluster progenitors at high redshift

David M. Nataf [1]⋆ Shunsaku Horiuchi [2] Guglielmo Costa [3,4]
Rosemary F. G. Wyse [1] Yuan-Sen Ting [5,6,7] Roland Crocker [8]
Christoph Federrath [8] and Yang Chen [4]

[1]*Department of Physics and Astronomy, The Johns Hopkins University, Baltimore, MD 21218, USA*
[2]*Center for Neutrino Physics, Department of Physics, Virginia Tech, Blacksburg, VA 24061, USA*
[3]*SISSA – ISAS – International School for Advanced Studies, Via Bonomea 265, I-34136 Trieste, Italy*
[4]*Dipartimento di Fisica e Astronomia Galileo Galilei, Università di Padova, Vicolo dell'Osservatorio 3, I-35122 Padova, Italy*
[5]*Institute for Advanced Study, Princeton, NJ 08540, USA*
[6]*Department of Astrophysical Sciences, Princeton University, Princeton, NJ 08544, USA*
[7]*Observatories of the Carnegie Institution of Washington, 813 Santa Barbara Street, Pasadena, CA 91101, USA*
[8]*Research School of Astronomy and Astrophysics, Australian National University, Canberra, ACT 2611, Australia*

ABSTRACT

Globular cluster progenitors may have been detected by *Hubble Space Telescope*, and are predicted to be observable with *James Webb Space Telescope (JWST)* and ground-based extremely large telescopes with adaptive optics. This has the potential to elucidate the issue of globular cluster formation and the origins of significantly helium-enriched subpopulations, a problem in Galactic astronomy with no satisfactory theoretical solution. Given this context, we use model stellar tracks and isochrones to investigate the predicted observational properties of helium-enriched stellar populations in globular cluster progenitors. We find that, relative to helium-normal populations, helium-enriched ($\Delta Y = +0.12$) stellar populations similar to those inferred in the most massive globular clusters, are expected, modulo some rapid fluctuations in the first ~ 30 Myr, to be brighter and redder in the rest frame. At fixed age, stellar mass, and metallicity, a helium-enriched population is predicted to converge to being ~ 0.40 mag brighter at $\lambda \approx 2.0 \, \mu m$, and to be 0.30-mag redder in the *JWST–NIRCam* colour ($F070W - F200W$), and to actually be fainter for $\lambda \lesssim 0.50 \, \mu m$. Separately, we find that the time-integrated shift in ionizing radiation is a negligible ~ 5 per cent, though we show that the Lyman-α escape fraction could end up higher for helium-enriched stars.

Key words: globular clusters: general.

1 INTRODUCTION

Globular cluster populations are predicted to trace the formation histories of galaxies. That is because mergers can both spur the formation of new globular clusters, and bring in additional clusters as part of the hierarchical assembly (Kruijssen et al. 2019a, b).

Ashman & Zepf (1992) and Zepf & Ashman (1993) proposed that the high pressure in the interstellar medium of merging, gas-rich systems could explain the mass–radius relation of old globular clusters, and the number and luminosity of young star clusters in currently merging systems. A supporting example is that of the major merging system Arp 220, which hosts at least 24 young star clusters with masses spanning a similar range as that of the Milky Way's 150+ globular clusters (Wilson et al. 2006). More

recently, the semi-analytic model of Muratov & Gnedin (2010) predicted that early mergers of smaller hosts create exclusively blue clusters, whereas subsequent mergers of more massive galaxies create both red and blue clusters, with the fraction of galactic stellar mass being in globular clusters declining from ~ 10 per cent at high redshift to ~ 0.1 per cent at present. Mandelker et al. (2018) used cosmological zoom-in simulations to propose that ~ 30 per cent of the Milky Way's metal-poor globular clusters originated from cold filamentary accretion, with the remainder accreted from mergers. Their scenario, which they predict to be most pronounced at a time corresponding to $z \sim 6$,[1] can account for the observed kinematics and spatial distribution of metal-poor globular clusters.

---

[1]Throughout this work, lower case '*z*' is used to denote cosmological redshift, and uppercase '*Z*' to denote the initial metals fraction of stars.

⋆ E-mail: dnataf1@jhu.edu

Globular clusters may also have significantly contributed to reionization. Boylan-Kolchin (2017, 2018) estimated that, for reasonable assumptions of the escape fraction, no less than 20 per cent of the ionizing sources with $M_{1500Å} \approx -12$ may have been globular clusters at $z \approx 4$. Zick, Weisz & Boylan-Kolchin (2018) have shown that for the progenitors of systems such as the Fornax dwarf galaxy, the globular clusters could account for a far greater share of their UV flux than their stellar mass fraction, if observed at the right times, since individual massive globular cluster stellar populations are formed in short-time intervals. Zick et al. (2018) also showed that ignoring this and related features can induce order-of-magnitude errors in abundance matching, between the first haloes to form stars and the galaxies observed in high-redshift data. Thus, a better understanding of globular cluster formation may be necessary to complete an inventory of ionizing photons during the reionization epoch.

Though the value of 20 per cent of the ionizing sources being globular clusters satisfies the trivial constraint of being less than 100 per cent, it is still disconcertingly high, as one can argue for changes to two of the assumptions made by Boylan-Kolchin (2018). These are that globular cluster stellar masses were not greater at the time of their birth than their present-day masses, and that there were no globular clusters that have since completely disassociated. These assumptions are not physically valid (Spitzer 1987; Fall & Zhang 2001), and thus the 20 per cent estimate is lower than a proper lower bound. That can be seen in fig. 5 of Zick et al. (2018), and is acknowledged in several sections of that work. If the initial masses of the globular cluster were merely ∼10 times higher, then their ionizing flux would exceed the measured luminosity function over the magnitude range $-19 \lesssim M_{1500} \lesssim -12$, where M_{1500} is the absolute magnitude of a source at $\lambda = 1500$ Å.

Kruijssen & Portegies Zwart (2009) estimated on dynamical grounds that the total stellar mass once formed in globular clusters is ∼40 times greater than their current total mass, with the losses due to both some globular clusters having lost some mass, and many having been completely disassociated. Renormalizing the 20 per cent estimate by this mass-loss argument shows that the estimates of Kruijssen & Portegies Zwart (2009) and Boylan-Kolchin (2018) are mutually exclusive, at a factor ∼10 level, if we assume the ionizing radiation field estimates of (Finkelstein 2016). Separately, Sollima & Baumgardt (2017) have measured the present-day stellar mass functions of 35 Galactic globular clusters spanning the range dn/d$m \propto m^{-1.89}$ to $m^{+0.11}$, with a median of $m^{-0.69}$. Their measured mass functions are tightly correlated with the ratio of the age to the half-mass relaxation times of the clusters, where that ratio can be called a dynamical age. That is the expectation if shallower mass functions originate from dynamical evaporation, in which the lower mass stars are expected to be preferentially lost over time due to mass segregation, superimposed on a universal initial mass function (Baumgardt & Makino 2003; Lamers, Baumgardt & Gieles 2013; Webb & Leigh 2015). Using these constraints, Sollima & Baumgardt (2017) estimate that ∼2 × 10^8 M$_\odot$ of Milky Way stars are evaporated members of the surviving globular clusters, which is some ∼7 times greater than the current integrated stellar mass of the Milky Way globular cluster system (Kruijssen & Portegies Zwart 2009), and comparable to the current literature consensus estimate for the total stellar mass of the halo of $(4-7) \times 10^8$ M$_\odot$ (Bland-Hawthorn & Gerhard 2016).

These dynamical arguments are now somewhat supported by chemical evolution arguments. Globular clusters host multiple populations differing in chemistry, which are typically assumed to be 'generations'. Typically, some approximately one-third of the stars in globular clusters have abundances that are consistent with the metallicity-dependent trends of the Milky Way halo, thick disk, and bulge (Carretta et al. 2009a), whereas the remaining two-thirds show various light-element trends, such as enrichment of sodium and aluminium and depletion of oxygen and magnesium (Carretta et al. 2009a; Johnson et al. 2017a, b; Nataf et al. 2019), and enrichment in helium (Norris 2004; Piotto et al. 2007). It is conventionally assumed – but not demonstrated – that the population showing anomalous abundances formed some unspecified time after the population showing normal abundances, from the gaseous ejecta of the first-generation stars. These form a 'first' and a 'second' generation. The chemical properties of multiple populations are correlated with the stellar mass and metallicity of the host globular clusters (Milone et al. 2017; Nataf et al. 2019).

If one assumes a standard initial stellar mass function and chemical yield values, the surviving globular clusters must have been no less than ∼10 times more massive at birth (Valcarce & Catelan 2011; Conroy 2012). That estimate results from requiring the ejecta of the asymptotic giant branch stars of the first generations to have sufficient mass to be recycled as the second generation, with its present-day number counts. This is referred to as the 'mass–budget problem'. There is currently no model in the literature that succeeds at accounting for each of the dynamical constraints, the abundance trends, and the mass–budget problem (Renzini 2013; Bastian & Lardo 2018). Though both dynamical and chemical arguments necessitate globular cluster mass-loss, the quantity of mass-loss has not been shown to be commensurate. There is no viable, general theory of globular cluster formation at this time, just a sea of unexplained observations and desperate phenomenology.

Martell & Grebel (2010) and Schiavon et al. (2017) used chemical abundance measurements of field stars to argue that a significant fraction, perhaps ∼50 per cent, of Milky Way stars with [Fe/H] ≤ −1 originated in globular clusters hosting multiple generations. That is in contrast to star formation today, which takes place in lower mass associations and open clusters. These do not show the abundance anomalies associated with globular clusters (Bragaglia et al. 2014; Cunha et al. 2015; Bragaglia et al. 2018). It has not been ascertained if this is predominantly due to stars ejected from surviving globular clusters, or from now fully disassociated globular clusters. That should eventually be straightforward to measure as the precision of chemodynamical tagging improves (Ting, Conroy & Goodman 2015).

Perhaps surprisingly, searches for the relevant abundance anomalies (Cabrera-Ziri et al. 2016; Martocchia et al. 2017) or age spreads (Cabrera-Ziri et al. 2014) in young star clusters in nearby locations such as the Large Magellanic Cloud with mass and size comparable to those of present-day Galactic globular clusters have yielded null results. The creation of multiple stellar generations in globular clusters may be a feature of the high-redshift universe. It has been demonstrated that young clusters do host stars with a large and unexplained spread in angular momentum (Bastian et al. 2016, 2018; Marino et al. 2018; Li et al. 2019), but at this time it is unknown if that phenomenon is related to that of chemically distinct populations in massive globular clusters. Separately, the theoretical investigation of Roy et al. (2019) showed that more rapidly rotating massive stars are expected to experience more and earlier dredge up, and thus shift to redder colours earlier in their evolution. It is also the case that lower metallicity massive stars are expected to have much faster rotation rates (Chiappini 2013). Given these factors, a separate study investigating the predicted effects of rotation on young massive clusters would be worthwhile.

In that case, directly constraining the nature of these systems' formation can only come from deep, precise imaging and spectroscopy.

Renzini ([2017](#)) has shown that globular cluster progenitors should be detectable with the *James Webb Space Telescope (JWST)* in each of the optical, near-infrared (near-IR), and mid-IR bands, even with modest exposure times of 10,000 seconds, or approximately 3 h. Deep observations can establish independent constraints on the initial masses of globular clusters, their formation history as a function of redshift, and the physical state of their host galaxies at the time of globular cluster formation, with the total numbers of globular clusters detected being a sensitive indicator of the initial mass function of globular clusters (Pozzetti, Maraston & Renzini [2019](#)). Pozzetti et al. ([2019](#)) computed more detailed estimates, and concluded that the total number counts of observed globular cluster progenitors would sharply constrain their initial mass function, independently of the formation redshift. We note that the first suggestion of such observations was that of Carlberg ([2002](#)), who predicted the luminosity function and clustering of globular cluster progenitors at high redshift.

The proposal that *JWST* (and eventually extremely large ground-based telescopes with adaptive optics) might constrain globular cluster formation models is supported by arguments that globular cluster progenitors might already have been observed with the *Hubble Space Telescope (HST)* (Bouwens et al. [2017](#); Vanzella et al. [2019b](#)). Vanzella et al. ([2019a](#)) have actually obtained spectra for one of these candidate clusters. It is at a redshift $z = 3.121$, has an estimated stellar mass $M \lesssim 10^7 \, M_\odot$, an effective radius smaller than 20 pc, and does indeed punch a hole through the surrounding medium to release some ionizing radiation.

There is a typo in the above paragraph, it should say z=2.37, not z=3.121, and the two references to Vanzella et al. (2019b) should be replaced by that here: https://ui.adsabs.harvard.edu/abs/2020MN RAS.491.1093V/abstract

In this paper, we investigate the predicted observable quantities of helium enrichment on future, high-redshift observations of globular cluster progenitors. We assume that globular clusters do not just undergo a single starburst, but typically two or more. The second generation is often enriched in helium, with the most massive globular clusters typically hosting second stellar generations with the largest enrichments in helium (e.g. Norris [2004](#); Piotto et al. [2007](#); Milone et al. [2017](#)). The most massive globular clusters are also expected to be the most easily observable (Renzini [2017](#); Pozzetti et al. [2019](#)), and it thus follows the most easily observable clusters will likely be those with higher stellar helium abundances. We thus explore and investigate the effect of helium enrichment on the evolution of high-mass stars using the best-available tracks and isochrones for this purpose, in combination with modelling of synthetic simple stellar populations.

The structure of this paper is as follows. In Section 2, we review some of the applications of stellar models in interpreting the properties of helium-enriched populations. In Section 3 and 4, we explore the effect of helium enrichment on stellar tracks of high-mass stars, and on combined simple stellar populations, respectively, which are due to helium-dependent shifts in the lifetimes of stars and their evolutionary tracks in the Hertzsprung–Russel diagram. In a brief segue, in Section 5, we explore the possibility that other factors may vary, such as the escape fraction of ionizing photons. We conclude in Section 6.

2 HELIUM-ENRICHED STELLAR MODELS

2.1 Theoretical primer

In the subsequent subsections, we will discuss various specific and detailed predictions of helium-enriched stellar models. Before doing

so, however, it is worth noting that the qualitative predictions have long been understood. It was Salpeter ([1952](#)), who discovered that helium fusion could be an important energy source for stars that had depleted their hydrogen, and Crawford ([1953](#)), who subsequently published the first stellar models for pure helium stars.

Helium-enriched stars are expected to be different from helium-normal stars due to, among other reasons:

(i) Being born with their main fuel source (hydrogen) being already partially depleted;

(ii) Their greater mean molecular weight, which makes nuclear fusion more efficient; and

(iii) Their reduced opacity, as helium has fewer electrons than hydrogen at fixed total mass.

These issues are discussed and explained in many standard textbooks on stellar structure and evolution (e.g. Kippenhahn & Weigert [1990](#); Boehm-Vitense [1992](#); Salaris & Cassisi [2005](#)).

2.2 Previous theoretical work on helium-enriched stellar populations

The effects of helium-enrichment on stellar models, largely driven by the need to model and understand observations of present-day Galactic globular clusters, has been predominantly discussed and explored at lower stellar masses. Among these:

2.3 Helium-enriched stellar models used in this investigation

In this investigation, we discuss the predictions for stars that are both higher mass and helium-enriched, given the context that high-redshift globular cluster progenitors may soon be observed in integrated light by *JWST*. To the best of our knowledge, this has not been explored in the literature. We used two sets of stellar models, which were treated differently. This combination allows for a few consistency checks to be implemented in this new predictive regime.

We primarily use a second set of models based on the PARSEC v1.2 code (Bressan et al. [2012](#); Tang et al. [2014](#); Chen et al. [2015](#)). A grid of stellar tracks densely samples the parameter of initial stellar masses up to $M_i = 300 \, M_\odot$, with bolometric corrections computed following the prescription of Chen et al. ([2019](#)). Three families of isochrones are constructed, with the metals fraction fixed to $Z = 0.017$ (the solar value) but the initial helium abundance set to $Y = 0.279$ (hereafter rounded to $Y = 0.28$), 0.33, and 0.40. These models do not include the asymptotic giant branch phase, and thus we are using them only to further probe the predicted properties of helium-enriched stellar populations in the first ~ 100 Myr, when the luminosities of higher mass stars dominate the flux budget. We also briefly discuss the evolution of core masses in these stars.

The mass-loss prescription for these tracks and isochrones are described by Chen et al. ([2015](#)). These assume the metals mixture of Caffau et al. ([2009](#)). The mass-loss prescription is a function of evolutionary phase and metallicity of the stars. This includes different prescriptions for the mass-loss during the blue supergiant phase (Vink, de Koter & Lamers [2000](#), [2001](#)), supergiants with $T_{\rm eff} \leq 12,000 \, K$ (de Jager, Nieuwenhuijzen & van der Hucht [1988](#)), and stars in the Wolf–Rayet phase (Nugis & Lamers [2000](#)).

Integrated stellar properties are computed directly from the isochrones. We adopt a Salpeter initial mass function (IMF) with slope $dN/dM \propto M^\alpha$ with $\alpha = -2.35$ (Salpeter [1955](#)). The total stellar mass is normalized to be $10^6 \, M_\odot$ over the mass range 0.5–$300 M_\odot$. Following the work of Renzini ([2017](#)), we assume that the

stars are formed with a uniform age dispersion spanning 3 Myr. Absolute magnitudes on the Vega system are computed for the bandpasses *F170W*, *F218W*, *F255W*, *F300W*, *F336W*, *F439W*, *F450W*, *F555W*, *F606W*, *F702W*, and *F814W* filter of the *WFC3 UVIS* imager on *HST*, and for the *F070W*, *F090W*, *F115W*, *F150W*, *F200W*, *F277W*, *F356W*, *F444W*, *F150W2*, and *F322W2* of the *NIRCam* imager on *JWST*. The same 10 *JWST* filters were recently selected in the related investigation of Pozzetti et al. (2019). The fluxes in the latter are computed both in the rest frame, and redshifted to $z = 0.10, 0.20, .., 0.90$ and $z = 1, 2, ..., 10$ using the cosmology calculator of (Wright 2006). The assumed cosmology is $H_0 = 69.6$, $\Omega_M = 0.286$, and $\Omega_\Lambda = 0.714$ with no curvature (Bennett et al. 2014).

We also make use of the stellar tracks of Bertelli et al. (2008, 2009). This second set of models is first used to enable a consistency and calibration check with the first, and also, because the broader range of input abundances available enable further tests of the effects of varying abundances. The input abundances include a broad range in the metals-mass fraction Z and the helium mass fraction Y, of which we use $\log Z/Z_\odot = -2.23, -1.23, 0, +0.37$ and $Y = 0.26$, 0.30, 0.34, and 0.40. These models assume the solar metals mixture of Grevesse & Noels (1993).

To compute integrated light estimates from these populations, we use the PEGASE.2 evolutionary synthesis code (Fioc & Rocca-Volmerange 1999) to investigate integrated properties of synthetic stellar populations. We replace the default stellar evolutionary stellar tracks with the He-rich tracks of Bertelli et al. (2009),[2] including the main-sequence, horizontal branch, and asymptotic giant branch tracks. We adopt a Salpeter IMF with slope $dN/dM \propto M^\alpha$ with $\alpha = -2.35$ over the mass range 0.5–$20\,M_\odot$ to match the availability of the Bertelli et al. (2009) tracks. With this setup, we follow the evolution of a stellar population of total initial mass $10^6\,M_\odot$ undergoing continuous star formation rate with of $50\,M_\odot\,yr^{-1}$, separately for $Y = 0.23$–0.4. The total duration of star formation is 20,000 years, and thus effectively instantaneous.

The main limitations to the models of Bertelli et al. (2009) are the coarseness of the mass grid at high masses, for which the available masses are $M/M_\odot = 8, 10, 12, 15, 20$, and the absence of models for stars with initial masses $M/M_\odot > 20$.

3 THE PREDICTED EFFECT OF ENRICHED HELIUM ON THE EVOLUTION OF SINGLE STARS

We show, in Fig. 1, the predicted evolution of high-mass stars at both standard and enriched initial helium abundance on the Herztprung–Russel diagram. In both cases, the more massive stars reach hotter temperatures, and are consistently more luminous at a fixed temperature. That continues the trend seen in low-mass models discussed in the previous section. In Fig. 2, we show different sets of information for the same stars – the cumulative radiated energy as a function of age. The predicted energy released is negligibly dependent on the initial helium abundance. For $M/M_\odot = 8$ stars, the $Y = 0.40$ star releases 6 per cent less total energy than the $Y = 0.28$ star, and for $M/M_\odot = 100$ stars, the reduction is 12 per cent. These shifts are smaller than the ~20 per cent reduction in total available fuel. We have verified that the two sets of isochrones yield consistent answers in the part of parameter space where they both have predictions.
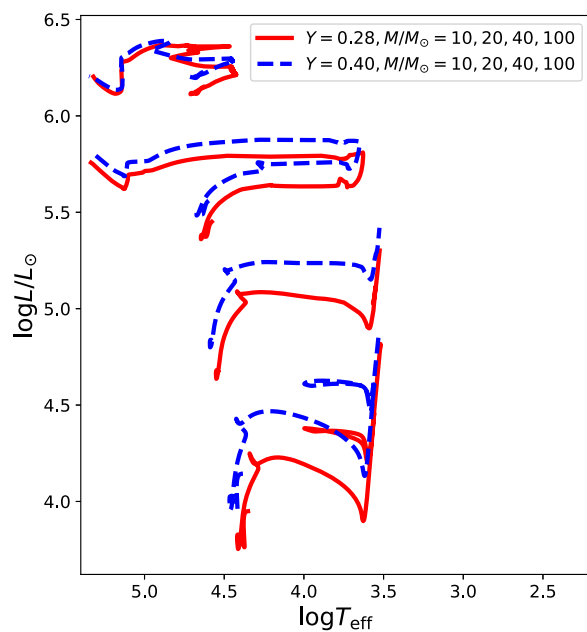
[2]http://cdsweb.u-strasbg.fr/cgi-bin/qcat?J/A+A/508/355

Figure 1. Predicted evolution of high-mass stars on the Hertzprung–Russel diagram. The helium-enriched stars are systematically bluer and brighter, mimicking the effect of higher mass at fixed helium. At fixed initial mass, helium-enriched stars live substantially shorter lives.
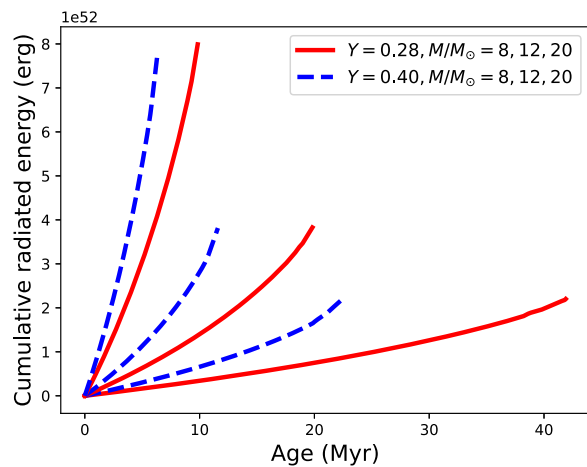

Figure 2. The cumulative radiated energy of high-mass stars, as a function of mass and initial helium abundance, versus age. The helium-enriched stars achieve comparable total radiated energy at fixed mass, but do so with a shorter lifetime. As in Fig. 1, this is true for both the 20–100 $M/M_\odot$ tracks computed using the PARSEC v1.2 code.

We show, in Fig. 3, the predicted lifetimes of high-mass stars as a function of mass and initial helium abundance. At fixed mass, stellar lifetime decreases with increasing initial helium abundance. That is due to three factors. The first is that helium-enriched stars are born with less hydrogen at fixed mass (by definition), and thus their main fuel source is already depleted. Secondly, the mean molecular weight is increased (as helium atoms are approximately four times heavier than hydrogen atoms), and thus the interior equilibrium temperature and thus luminosity increases as well. Finally, the reduction in the total number of free electrons per unit mass reduces the internal opacity of the star.
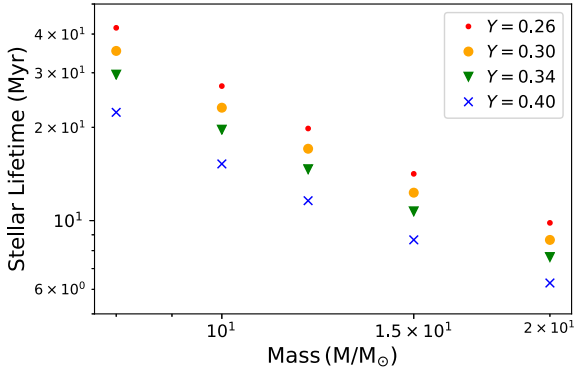
Figure 3. The predicted stellar lifetimes are shown as a function of stellar mass and initial helium abundance.

A multivariate least-squares fit of the stellar lifetime for tracks from Bertelli et al. (2008, 2009) satisfying $8 \leq (M/M_\odot) \leq 20$ and $0.26 \leq Y \leq 0.40$ yields the following scaling relation for the lifetime as a function of stellar mass:

$$\tau \approx (27\,\text{Myr}) \left(\frac{M}{10\,\text{M}_\odot} \right)^{-1.49} \times \exp\left[-3.82(Y - 0.26)\right]. \qquad (1)$$

The typical error in our coverage of this parameter space is less than 5 per cent.

Equation (1) is, unsurprisingly, not simply the continuation of fits done at the lower mass regime (Nataf et al. 2012; Karakas 2014). The effects of both mass and helium on the stellar lifetime are decreased at these higher stellar masses. Nevertheless, though the effect of helium enrichment on stellar lifetime is lessened relative to lower mass stars, it is still present. For example, the lifetime of the $10\,\text{M}_\odot$, $Y = 0.26$ star is 27 Myr, similar to that of the $7.5\,\text{M}_\odot$, $Y = 0.40$ star.

If one assumes equation (1), an initial mass function of $dn/dm \propto m^{-2.35}$ for masses $M/M_\odot \leq 100$, and the same total stellar mass formed, the total amount of material that was in stars that have become remnants by $t = 27$ Myr will be $\sim$19 per cent higher for the $Y = 0.40$ population than for the $Y = 0.26$ population, and the total number of remnants will be $\sim$50 per cent higher.

3.1 The separate effects of helium and metallicity on high-mass stellar tracks

In this investigation, we are predominantly using tracks and isochrones of solar metallicity. Our results should be robust to this choice of metallicity as long as the predicted photometric observables of stellar populations have negligible cross-terms in their dependence on metallicity and initial helium abundance.

We verify this in two different ways. We first compute the coefficients of equation (1) for a set of tracks shifted to lower metallicity by $\Delta \log Z = 1.23$ dex – we find that the coefficients shift downward by ~ 7 per cent. The same approximate non-covariance of the effects of metallicity and helium has already been demonstrated for predictions of lower mass stars (Karakas et al. 2014). We also similarly compute the dependence of the cumulative integrated luminosity – energy – released by stars as a function of stellar mass and initial helium abundance. Here, a shift to lower metallicity of $\Delta \log Z = 1.23$ dex results in shifts to the coefficients of less than 3 per cent or less.

The assumption that the effects of metallicity and helium on predicted photometric observables of young stellar populations is

non-covariant is thus sufficiently supported for this work. However, further study over a broader metallicity range will likely be warranted in the future.

4 THE PREDICTED EFFECT OF ENRICHED HELIUM ON THE INTEGRATED LIGHT OF STARBURSTS

The previous section's discussion of high-mass, helium-enriched stellar tracks can facilitate our understanding of why helium enrichment might matter. However, we do not expect *JWST* to observe isolated massive helium-enriched stars, rather it will observe integrated light from populations of these stars.

In the following, we analyse the predicted effects of a globular cluster progenitor being helium-enriched at fixed mass, age, and metallicity. This is intended to isolate the effect of helium. In practice, helium-enriched stars are expected to have been formed in lesser numbers than helium-normal stars (D'Ercole et al. 2008; Valcarce & Catelan 2011; Conroy 2012

After Conroy 2012, add a reference to this paper: https://ui.adsabs.harvard.edu/abs/2017MNRAS.470..977L/abstract), and the fraction of helium-enriched stars and the amplitude of their helium enrichment may be correlated with metallicity (Carretta et al. 2009a; Milone et al. 2017). Conversely, the helium-enriched populations might actually be slightly younger than the helium-normal populations, if they formed from the gas of the ejecta of the helium-normal stars, in which case they could temporarily dominate the flux budget of a globular cluster progenitor. We cannot account for that factor as, at this time, the age difference between helium-normal and helium-enriched populations remains uncertain.

4.1 The predicted effect of enriched helium during the first 150 Myr

We have computed the integrated magnitudes and colours of the helium-normal and helium-enriched populations for for 12 *HST* filters in the rest frame, and for 10 *JWST–NIRCam* filters at 20 different redshifts. We show, in Fig. 4, 20 predicted differences in rest-frame predicted colours and magnitudes between the helium-normal and helium-enriched populations. We then show a selected subsample of predicted differences at various redshifts in Fig. 5. There is no clear and simple statement that can be written as to the first-order difference between the helium-normal and helium-enriched populations, and what statements can be written are a function of age. We summarize the age-specific trends as follows:

(i) In the first 5–10 Myr, the helium-enriched populations are predicted to be brighter at all wavelengths. That is due to their most massive stars more rapidly burning through their fuel.

(ii) There are several fluctuations in the period spanning 5 Myr after the starburst. The helium-enriched stars reach their red loops earlier, and are thus briefly much brighter. For example, at *F200W* the $Y = 0.40$ starburst is expected to be $\sim$1.6 mag brighter at $t \sim$ 5 Myr, which then reverses as the most massive helium-enriched stars die earlier, and the helium-normal stars then also reach their red loops.

(iii) Fluctuations continue in the period spanning 30–50 Myr after the starburst, but the differences in magnitudes and colours are mostly small.

(iv) From 50 Myr onward, the trends are more stable. The helium-enriched populations are fainter $\lambda \lesssim 5000$ Å, and brighter
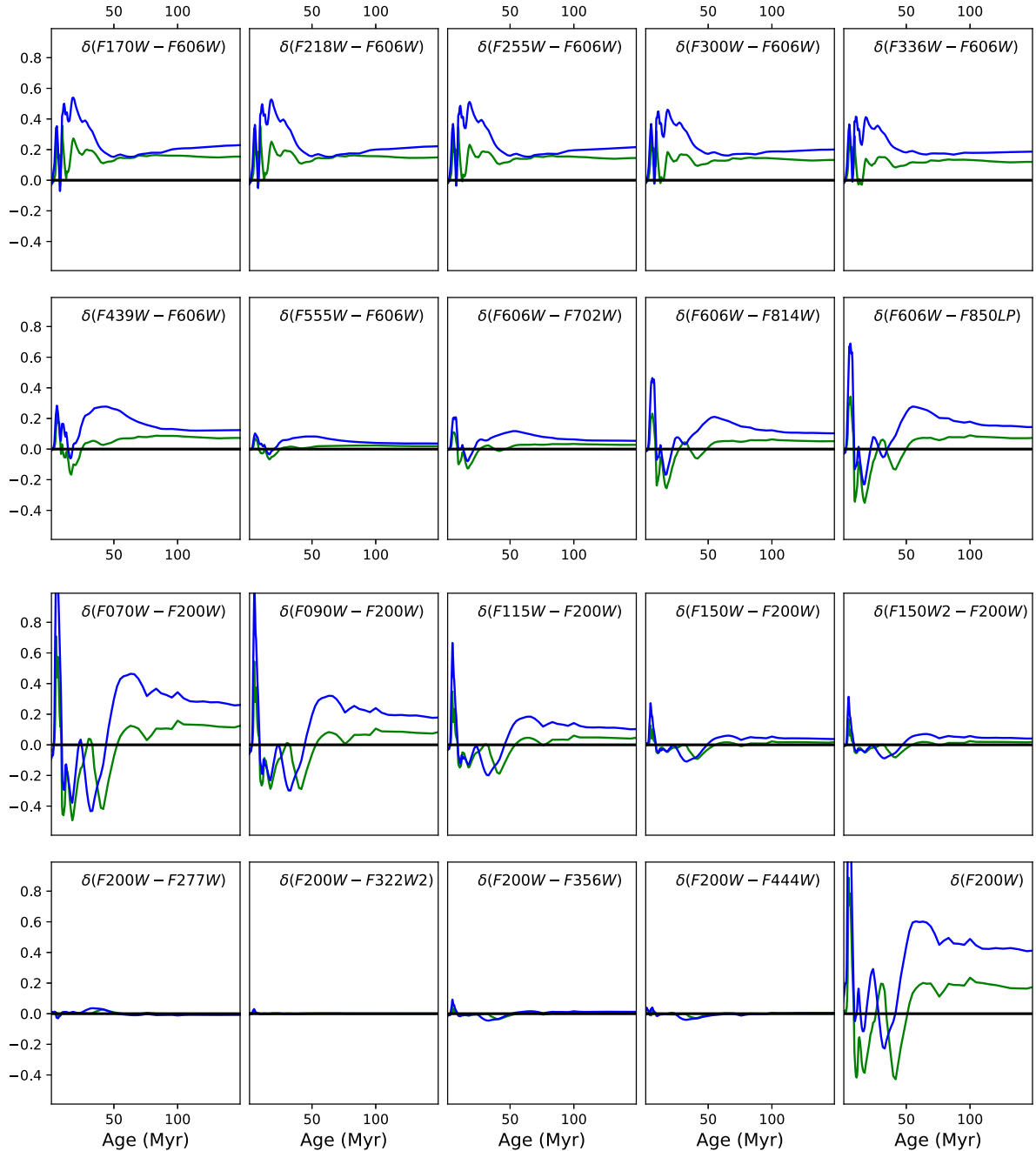
Figure 4. Difference in predicted rest-frame colours for the helium-enriched ($Y = 0.40$ in blue, $Y = 0.33$ in green) relative to helium-normal ($Y = 0.28$) populations as a function of age in the first 19 panels, with the difference in *JWST–NIRCam F*200*W* magnitude shown in the bottom right-hand panel. A positive value denotes the helium-enriched population being more red or more bright in the given filter combination.

at longer wavelengths, with brightness offset increasing at longer wavelengths. The $Y = 0.40$ population would converge to being $\sim$0.15 brighter in *F*070*W*, $\sim$0.30 brighter in *F*115*W*, and $\sim$0.40 brighter in *F*200*W*.

The origin of these rapid bolometric fluctuations for populations with $5 \lesssim \tau/\text{Myr} \lesssim 30$ can be discerned from Fig. 6. We show, in the bottom panel, the fraction of the total luminosity predicted to come from stars colder than $T_{\text{eff}} \leq 10,000\,K$ as a function of age. That fraction increases rapidly at $\tau \approx 4$ Myr, decreases again at $\tau \approx 12$ Myr, before then increasing and levelling off. The first increase

corresponds to the emergence of a red extension to the Hertzsprung–Russell diagram, which is present in the $\tau = 7$ Myr population, but not in that of the $\tau = 3$ Myr population. Similarly, there is a blue loop in the $\tau = 11$ Myr population, but not in the $\tau = 7$ Myr population. The effect of these rapid changes may increase the uncertainties in the eventual parameter estimates of globular cluster progenitors. In practice, our assumed age spread of $\Delta \tau = 3$ Myr may prove to be an underestimate for the progenitors of the most massive globular clusters. A larger $\Delta \tau$ would have the effect of reducing these fluctuations.
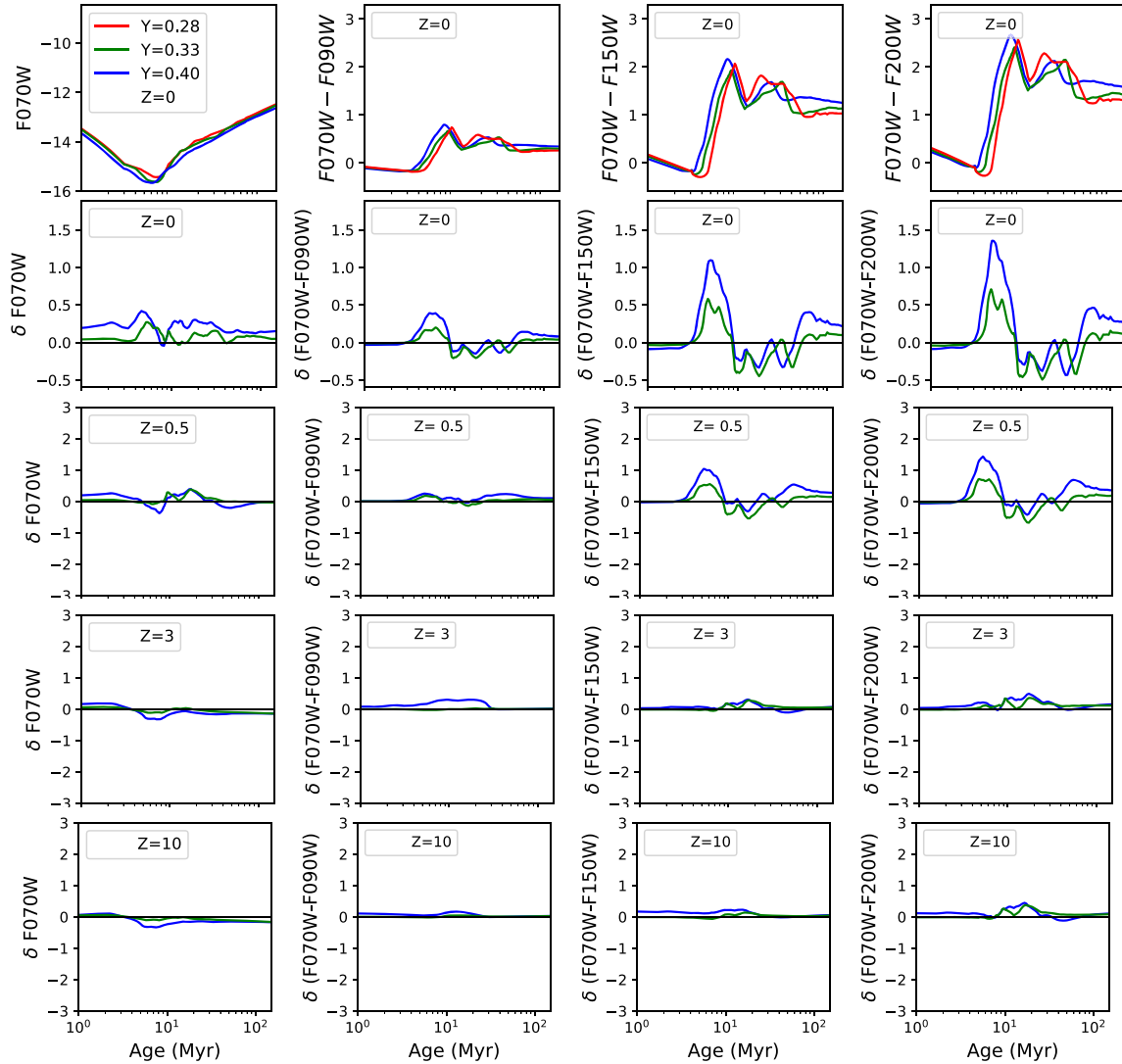
Figure 5. Top panel: a sample of rest-frame magnitudes and colours for the helium normal ($Y = 0.28$ in red), moderately helium enriched ($Y = 0.33$ in green), and extremely helium enriched synthetic populations ($Y = 0.40$ in blue). Bottom four panels: the difference between the magnitude and colours of the moderately helium-enriched ($Y = 0.33$ in green) and extremely helium-enriched synthetic populations ($Y = 0.40$ in blue) relative to that of the helium-normal population at four different cosmological redshifts. Here, positive values denote the helium-enriched population is brighter in the specified magnitude, or redder in the specified colour.

We show, in Fig. 7, how the differences between the helium-normal and helium-enriched populations continue through to $\tau = 160$ Myr. There are still some variations, but they are smaller than they were for ages $\tau \lesssim 30$ Myr. The helium-enriched population, to first order, continuously gets an additional 10 per cent of its integrated luminosity from stars with $T_{\rm eff} \leq 10,000 \, K$. The time-dependent and redshift-dependent predictions for globular cluster progenitors in the *JWST* bandpasses are listed in Table 1.

That the helium-enriched populations converge to being cooler, and thus redder in most filter combinations, may be counterintuitive, as the general literature on helium-enriched models, discussed in Section 2, often refers to how the tracks of individual helium-enriched stars are generally hotter than those of helium-normal stars at fixed initial mass and evaluated at the same evolutionary phase, with this shown again in Fig. 1. The shift to redder integrated colours occurs due to the fact that helium-enriched populations evolve faster, and thus they will contain proportionately more red

giants, at earlier times. We use the cumulative, integrated flux for the F170*W* bandpass as a proxy for the ionizing radiation, which we plot in Fig. 8. The helium-enriched populations are predicted to emit more of these (nearly)-ionizing photons – but only for the first ∼5 Myr. Subsequent to this, the cumulative radiation at these wavelengths is expected to be slightly ($\lesssim 5$ per cent) lower..

5 OTHER POSSIBLE SYSTEMATICS WITH YOUNG, HELIUM-ENRICHED STELLAR POPULATIONS

5.1 The effect of elevated helium abundance on the model atmospheres of stars

The prediction of ionizing radiation from the preceding section does not trivially follow from stellar theory. As discussed previously, a
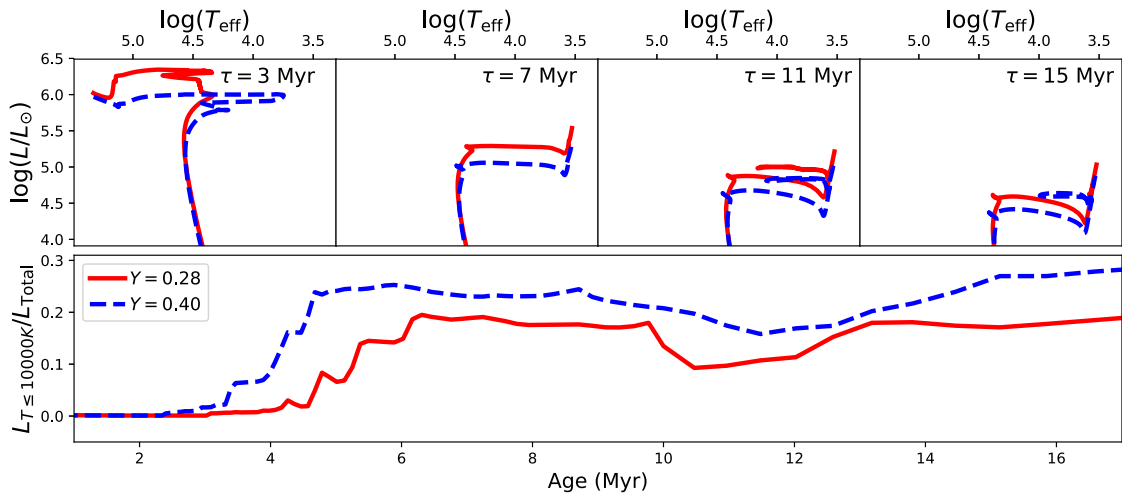
Figure 6. The sudden emergence of red and blue loops cause rapid fluctuations in the predicted bolometric output of stellar populations, between the ages of 3 and 15 Myr. Top panels: Isochrones for the helium-normal and helium-enriched populations for four representative ages. Bottom panels: the fraction of total luminosity from stars with $T_{eff} \leq 10,000 K$ as a function of age.
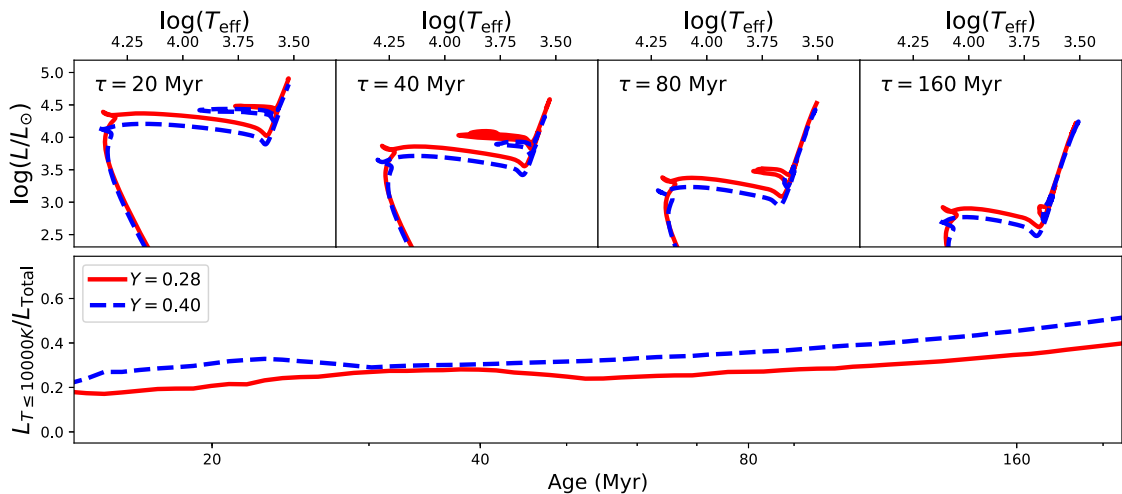
Figure 7. Same as Fig. 6, but for later ages, with the ages in the bottom panel plotted logarithmically. At these later ages, the differences between different stellar populations are a more stable function of time.

shift in Y leads to shifts in T_{eff}, and $\log g$ at fixed age, metallicity, and stellar mass. The stellar models used in this work have computed this shift, and have also assumed a mapping, from model atmospheres and synthetic spectra, to convert atmospheric parameters to various bandpass-dependent fluxes. However, this mapping might itself depend on Y, if the atmospheric structure depends on Y. We explore this issue here.

It is conceivable that the increased helium abundance could modify the atmospheric opacity of hotter stars. Among other changes, the decreased abundance of hydrogen necessitates a decreased stellar opacity to radiation that could contribute to the reionization of the universe.

We thus computed synthetic spectra for several cases. We first discuss the following four: $(\log T_{eff}, \log g) = (4.3899\ 3.8718)$ and $(4.4716\ 3.9959)$, for $Y = 0.26, 0.40$. We use the models of Kurucz (1970, 1993, 2005, 2013), Kurucz & Avrett (1981). Each model atmosphere assumes $\log (Z/Z_\odot) = -1.23$ on the abundance scale of Asplund et al. (2009). The temperature and gravity values are taken from the helium-normal and helium-enriched tracks. Without

correcting for atmospheric effects, the helium-enriched stars will automatically emit more ionizing radiation as they reach higher surface temperatures (Fig. 1). We find that the models predict an ∼1 per cent increase in total flux in the 1000 Å $\leq \lambda \leq$ 1500-Å range.

We also compute model atmospheres at $(\log T_{eff}, \log g) = (4.3899\ 3.8718)$ with both an α-enhanced, and a CNONa-extreme mixture, which is expected for the most helium-enriched globular cluster populations. Both mixtures have shifts of $+0.40$ dex in the α-abundances, and the second mixture has shifts of $-0.60, +1.80, -0.80, +0.80$ dex in the respective abundances of CNONa. The elemental abundance mixtures are respectively taken from Pietrinferni et al. (2006b) and Pietrinferni et al. (2009). We find that the models predict an ∼0.1 per cent increase in total flux in the 1,000 Å $\leq \lambda \leq$ 1500-Å range for the CNONa mixture, relative to the α-enhanced mixture. These effects are thus predicted to be negligible.

We note that the estimates of this subsection apply only to massive main-sequence stars that still have their birth composition, and that have surface temperatures colder than 30,000 Kelvin. Readers

Table 1. A subsample of predicted magnitude differences between a helium-enriched ($Y = 0.40$) and helium-normal population ($Y = 0.28$), as a function of population age and cosmological redshift z. Here, a positive value of Δmag means that the helium-enriched population is brighter. A version of this table which has denser sampling in age and redshift and covers 10 *JWST* bandpasses is available in the online addition.

| $\log(t/\mathrm{Myr})$	z	$\Delta F070W$	$\Delta F090W$	$\Delta F200W$
−1.00	0.0	0.16	0.13	0.07
−0.60	0.0	0.17	0.13	0.07
−0.20	0.0	0.18	0.15	0.09
0.20	0.0	0.22	0.20	0.16
0.60	0.0	0.30	0.45	1.01
1.00	0.0	0.21	0.10	− 0.04
1.40	0.0	0.25	0.26	0.23
1.80	0.0	0.14	0.28	0.60
−1.00	0.3	0.16	0.17	0.07
−0.60	0.3	0.16	0.17	0.07
−0.20	0.3	0.17	0.18	0.09
0.20	0.3	0.22	0.23	0.14
0.60	0.3	0.14	0.29	0.89
1.00	0.3	0.18	0.22	− 0.00
1.40	0.3	0.12	0.25	0.25
1.80	0.3	− 0.06	0.13	0.55
−1.00	10.0	0.48	0.32	0.16
−0.60	10.0	0.48	0.32	0.16
−0.20	10.0	0.50	0.33	0.16
0.20	10.0	0.42	0.33	0.20
0.60	10.0	0.06	0.14	− 0.01
1.00	10.0	0.86	0.72	− 0.10
1.40	10.0	2.73	0.73	− 0.10
1.80	10.0	− 0.14	− 0.25	− 0.13
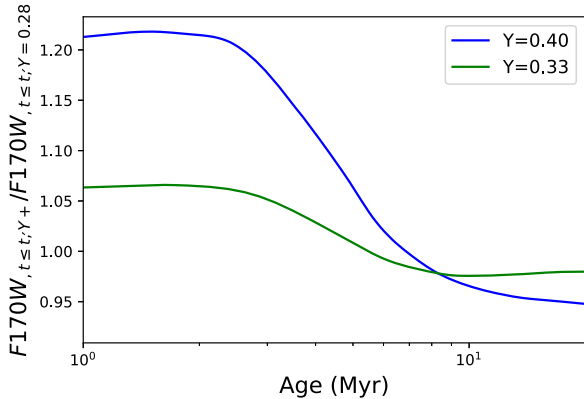
Figure 8. The predicted cumulative ratio of flux in the *F*170*W* filter, which we use as a proxy for ionizing flux, as a function of time, for the $Y = 0.40$ and 0.33 populations relative to the $Y = 0.28$ population. The predicted cumulative ionizing flux from the helium-enriched populations is similar to that of the helium-normal population.

interested in the effects at higher surface temperatures, and for massive stars with even more extreme CNO and He abundances due to evolution from factors such as internal mixing, are referred to Roy et al. (2019).

5.2 The plausibility of a higher Lyman-α escape fraction

The recent work of Boylan-Kolchin (2018) assumes that the escape fraction of ionizing radiation from globular clusters was $f_{esc}(t < t_{SNeII}) = 0$ and $f_{esc}(t > t_{SNeII}) = 1$. That is consistent with earlier

work arguing for an escape fraction close to unity (Ricotti 2002, 2004). The assumption of a high escape fraction after the supernovae explosions is not simply the heuristic argument that the shock of the explosions should drive out the gas. It is also due to measurements showing that second generations of globular clusters have little or no iron enrichment (Carretta et al. 2009b). Even in the case of the metal-diverse globular cluster ω Cen (NGC 5139), it can be estimated that 99.8 per cent of the supernovae ejecta were lost from the cluster (Renzini 2013). That estimate arises from the fact that though some stars in ω Cen have higher metallicities, they are not sufficiently high to account for all of the core-collapse supernovae of the more metal-poor stars in that cluster. This demonstrates that the supernovae ejecta were not held on to, and thus makes it unlikely that the remaining initial gas was held on to as well, as the two should be mixed at some level.

A prediction that is at odds with the assumptions of Boylan-Kolchin (2018) is that from the detailed simulations of Paardekooper, Khochfar & Dalla Vecchia (2015). The middle panel of their Fig. 5 shows the distribution of escape fraction as a function of stellar mass and redshift. The typical escape fraction of ionizing photons for systems with $M/M_\odot = 10^6$ is $f_{esc} \approx 0.01$. We note that the scatter is large in all displayed bins of redshift and star formation history, though the prediction of f_{esc} is that it will virtually always be lower than 10 per cent for $M/M_\odot \lesssim 10^7$.

Another result of Paardekooper et al. (2015) that is of interest to this study is that shown in their Fig. 3. The escape fraction of ionizing radiation is (unsurprisingly) predicted to be a decreasing function of increasing hydrogen column density N_H, for all redshifts and all star formation histories. A ∼10,000-fold increase in N_H results in a ∼100-fold decrease in f_{esc} (with substantial scatter).

This trend may be relevant for helium-enriched second generations, if their surrounding interstellar medium is also enriched in helium and correspondingly deficient in hydrogen. The opacity to Lyman-α photons would be reduced, since helium is effectively transparent to nearly all stellar radiation. Helium is not just a noble gas, but the noblest of them all. The first ionizing potential of helium is 24.62 eV, the highest of all of the elements, and some ∼80 per cent higher than that of hydrogen. The Lyman-α escape fraction of second-generation globular cluster starbursts should thus be increased.

This argument assumes that the efficiency of converting gas into stars does not change as the helium-to-hydrogen ratio changes. This may be incorrect – Herwig et al. (2012) argue in their Section 4.2.3 that gas enriched in He, N, Na, and depleted H, C, O, and Ne, as found in extreme globular cluster populations, would have a radiative cooling coefficient that is up to 0.50 dex higher than gas with a canonical composition, at fixed total metallicity. That is approximately equivalent to an increase of 1 dex in the total metallicity of the gas. We ignore this caveat here, and thus our estimate of increased ionizing flux is an underestimate, as the gas may be depleted in total mass in addition to being depleted in hydrogen.

Given that the number of hydrogen atoms is proportional to the mass in hydrogen of the star-forming cloud, the relationship between the optical depth of the first (τ_{GenI}) and of the second (τ_{GenII}) stellar generation should go as

$$\tau_{GenII} \approx \left(\frac{1 - Y_2}{0.75} \right) \tau_{GenI}, \qquad (2)$$

where Y_2 is the helium mass fraction of the second generation. The helium mass fraction inferred in the most massive globular clusters,
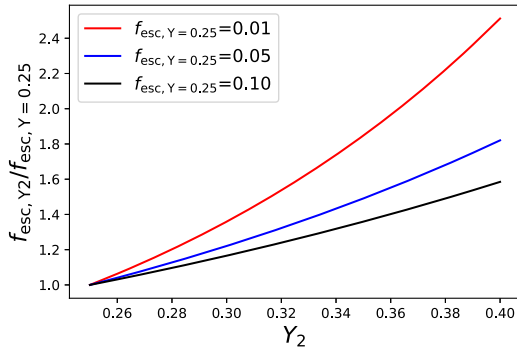
Figure 9. The fractional increase of the escape fraction of the second-generation relative to the first generation, $f_{\rm esc, GenII}/f_{\rm esc, GenI}$, as a function of the helium-mass fraction of the second generation (Y_2), and the escape fraction of the first generation ($f_{\rm esc, GenI}$).

$Y = 0.40$, would thus result in a fractional decrease of the optical depth of $(1 - 0.6/0.75) = 1 - 0.80 \rightarrow 20$ per cent.

The definition relating the optical depth to the escape fraction $f_{\rm esc}$ is

$$e^{-\tau} \equiv f_{\rm esc}. \tag{3}$$

It follows that a 1 per cent escape fraction for the first generation will translate to one as high as 2.5 per cent for the second generation, and that a 10 per cent escape fraction for the first generation will translate to one as high as 16 per cent for the second generation. Indeed, the fractional increase of the escape fraction goes as

$$\frac{f_{\rm esc,GenII}}{f_{\rm esc,GenI}} = \exp\left(\left[\frac{Y_2 - 0.25}{0.75}\right] \log f_{\rm esc,GenI}\right). \tag{4}$$

We show the fractional increase in escape fraction as a function of the initial escape fraction $f_{\rm esc, GenI}$ and the helium mass fraction of the second generation in Fig. 9.

It thus appears unlikely that the peculiar physics of helium-enriched stellar populations are a substantial perturbation on the reionization budget. Their escape fraction will only be substantially increased in the regime of high opacity, where there are few photons escaping in any case. However, prior calculations of $f_{\rm esc}$ for globular cluster progenitors predict values close to unity (Ricotti 2002, 2004), and thus the change would be negligible. It was also shown in the previous section that their cumulative ionizing flux will only be marginally increased.

5.3 Variations in initial helium abundance and the predicted final core masses of massive stars

We show, in Fig. 10, the predicted final helium core masses and carbon–oxygen core masses as a function of initial mass and varying initial helium abundance. These are the values predicted by the PARSEC v1.2 isochrones.

The predictions are for a substantial increase in the final helium-core mass, and a modest increase in the final carbon–oxygen core mass, as the initial helium abundance is increased. This continues the trend, predicted for lower mass stars, of larger mass remnants as a function of initial mass for helium-enriched populations (Karakas et al. 2014; Chantereau et al. 2017).

Our findings are thus qualitatively consistent with the argument of Karakas & Shingles (2017), that helium enrichment could shift the mass threshold for core-collapse supernovae at fixed metallicity. We cannot ascertain quantitative consistency at this time as this would
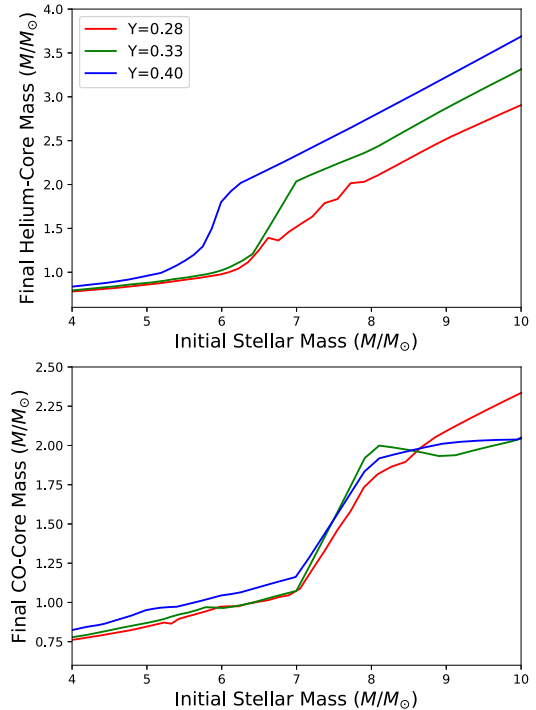

Figure 10. The final masses of Helium-core (top panel) and carbon-oxygen core (bottom panel) as a function of initial stellar mass and initial helium abundance, as predicted by the PARSEC v1.2 isochrones.

require a separate investigation. However, this has the potential to contribute an offset to the integral of ionizing flux, as the supernovae themselves contribute a lot of ionizing radiation, and more massive cores at fixed initial mass and fixed initial mass function would necessitate a greater number of core-collapse supernovae.

6 DISCUSSION AND CONCLUSION

In this work, we have investigated the predicted effects of higher initial helium abundances in the flux of massive globular cluster starbursts. We have done this using two sets of tracks and isochrones. We predominantly made use of tracks and isochrones that computed for this work using the PARSEC v1.2 code (Bressan et al. 2012; Tang et al. 2014; Chen et al. 2015). We also used the tracks and isochrones from the works of Bertelli et al. (2008, 2009) as a consistency check.

We found that at fixed metallicity, age, and total stellar mass, helium-enriched stellar populations are expected to be redder from ~50 Myr onward, with rapid fluctuations taking place before that time. The helium-enriched ($\Delta Y = 0.12$) population then converges to being fainter for $\lambda \lesssim 0.50\,\mu m$, and up to 0.40 mag brighter at $\lambda \approx 2.0\,\mu m$.

Given that the first set of observations of globular cluster progenitors will likely be very coarse, we do not expect the effect of helium abundance variations to be immediately disentangled. A likelier outcome is that, if a helium-enriched population is observed, it will be misconstrued as having the wrong age, metallicity, and mass. However, it is also the case that there will often be no satisfactory fit if observations are made in a sufficient number of bandpasses, which may result in an interpretation of helium enrichment.

In Section 5, we explored some other possible effects. We found that the amount of radiation capable of ionizing hydrogen could be shifted higher, but only marginally so, due to two effects. First, the

O-stars should themselves have a slightly lower opacity to ionizing radiation, but this effect turned out to be very small. Secondly, the interstellar medium surrounding these globular clusters might itself be depleted in hydrogen due to being enhanced in helium, and thus the escape fraction would be shifted higher. A potentially larger effect is that of the higher final core masses predicted by the PARSEC v1.2 models, which would suggest more massive remnants, and a potentially greater number of core-collapse supernovae.

There are several additional sources of systematic uncertainty that we have not accounted for. We discuss four of these:

(i) We assumed that helium-normal and helium-enriched stellar populations would form massive stars with the same initial mass function. This assumption can be a functional hypothesis, but it is without empirical support. However, the IMF is believed to be primarily a result of turbulent fragmentation, moderated by magnetic fields and stellar feedback from jets and radiation (Padoan & Nordlund 2002; Hennebelle & Chabrier 2009; Hopkins 2012; Federrath et al. 2014; Krumholz & Federrath 2019) and is therefore unlikely to depend on the effects of helium enrichment discussed here.

(ii) Similarly for the binary fraction, which could create more (or fewer) massive stars and altered evolutionary channels by means of mergers and mass transfers. There is evidence that the lower mass stars of the second generations of globular clusters have lower binary fractions (D'Orazi et al. 2010; Lucatello et al. 2015), but the implications for the binary fraction at higher masses are uncertain.

(iii) Similarly for rotation, which we neglected. We did not explore whether rotation would have a different evolutionary effect on helium-enriched stars than it does on helium-normal stars, nor whether we should expect the distribution of rotation rates to be a function of helium abundance. Variations in the rotation would have an effect, as increased rotation results in increased luminosity at fixed metallicity and mass for massive stars (Brott et al. 2011). Rotation also has an effect on the observed $T_{\rm eff}$, magnitudes and colours of massive stars in a manner that depends on the inclination angle between the star's rotation axis and the line of sight to the star (Girardi et al. 2019). There is evidence for a rotational dichotomy in intermediate-age clusters in the Large Magellanic Cloud (Bastian et al. 2018; Goudfrooij et al. 2018), but it is not known if this would have also been the case in the massive stars of globular clusters, and how it would have mapped on to populations with different abundances.

(iv) Mass-loss will have a substantial effect. This can be easily discerned by, for example, inspecting Figs 6 and seeing the magnitude variations in the 0–20 Myr range. This will undoubtedly challenge attempts at interpreting *JWST* data – there are no empirical constraints on mass-loss for massive stars with [Fe/H] ≤ -1.0, as there are no such stars in the Local Group. Further, the assumption that mass-loss is similar for massive helium-normal and helium-enriched stars may not be correct – it is seemingly incorrect at low masses. The relative paucity of abundance anomalies on the asymptotic giant branches of globular clusters (Norris et al. 1981; Campbell et al. 2013; MacLean et al. 2016) suggests that mass-loss may be increased in helium-enriched stars, causing those stars to bypass the asymptotic giant branch and go straight to the hot horizontal branch stars. Those are the AGB-manqué stars, originally postulated by Greggio & Renzini (1990), to explain the excess ultraviolet luminosity of metal-rich elliptical galaxies (Faber 1983; Burstein et al. 1988; Goudfrooij 2018).

There is thus a need for further theoretical work in the coming years, as observations of young, massive star clusters at high-redshift come in. These will augment the current samples (from lensed systems, Bouwens et al. 2017; Vanzella et al. 2019a), by at least two orders of magnitude (Pozzetti et al. 2019). Characterizing such systems, quantifying their contribution to reionization, and relating them to the populations of old globular clusters seen today may become one of the major emerging fields of astronomy.

REFERENCES

Ashman K. M., Zepf S. E., 1992, ApJ, 384, 50
Asplund M., Grevesse N., Sauval A. J., Scott P., 2009, ARA&A, 47, 481
Bastian N. et al., 2016, MNRAS, 460, L20
Bastian N., Lardo C., 2018, ARA&A, 56, 83
Bastian N., Kamann S., Cabrera-Ziri I., Georgy C., Ekström S., Charbonnel C., de Juan Ovelar M., Usher C., 2018, MNRAS, 480, 3739
Baumgardt H., Makino J., 2003, MNRAS, 340, 227
Bennett C. L., Larson D., Weiland J. L., Hinshaw G., 2014, ApJ, 794, 135
Bertelli G., Girardi L., Marigo P., Nasi E., 2008, A&A, 484, 815
Bertelli G., Nasi E., Girardi L., Marigo P., 2009, A&A, 508, 355
Bland-Hawthorn J., Gerhard O., 2016, ARA&A, 54, 529
Boehm-Vitense E., 1992, Introduction to Stellar Astrophysics. Vol. 3: Stellar structure and evolution, Cambridge Univ. Press, Cambridge
Bono G., Cassisi S., Zoccali M., Piotto G., 2001, ApJ, 546, L109
Bouwens R. J., van Dokkum P. G., Illingworth G. D., Oesch P. A., Maseda M., Ribeiro B., Stefanon M., Lam D., 2017, preprint (arXiv:1711.02090)
Boylan-Kolchin M., 2017, MNRAS, 472, 3120
Boylan-Kolchin M., 2018, MNRAS, 479, 332
Bragaglia A., Sneden C., Carretta E., Gratton R. G., Lucatello S., Bernath P. F., Brooke J. S. A., Ram R. S., 2014, ApJ, 796, 68
Bragaglia A., Fu X., Mucciarelli A., Andreuzzi G., Donati P., 2018, A&A, 619, A176
Bressan A., Marigo P., Girardi L., Salasnich B., Dal Cero C., Rubele S., Nanni A., 2012, MNRAS, 427, 127
Brott I. et al., 2011, A&A, 530, A115
Burstein D., Bertola F., Buson L. M., Faber S. M., Lauer T. R., 1988, ApJ, 328, 440
Cabrera-Ziri I., Bastian N., Davies B., Magris G., Bruzual G., Schweizer F., 2014, MNRAS, 441, 2754
Cabrera-Ziri I., Lardo C., Davies B., Bastian N., Beccari G., Larsen S. S., Hernandez S., 2016, MNRAS, 460, 1869

Caffau E., Maiorca E., Bonifacio P., Faraggiana R., Steffen M., Ludwig H. G., Kamp I., Busso M., 2009, A&A, 498, 877

Campbell S. W. et al., 2013, Nature, 498, 198

Carlberg R. G., 2002, ApJ, 573, 60

Carretta E. et al., 2009a, A&A, 505, 117

Carretta E., Bragaglia A., Gratton R., D'Orazi V., Lucatello S., 2009b, A&A, 508, 695

Cassisi S., Salaris M., 1997, MNRAS, 285, 593

Chantereau W., Charbonnel C., Meynet G., 2017, A&A, 602, A13

Chantereau W., Usher C., Bastian N., 2018, MNRAS, 478, 2368

Chen Y. et al., 2019, A&A, 632, A105

Chen Y., Bressan A., Girardi L., Marigo P., Kong X., Lanza A., 2015, MNRAS, 452, 1068

Chiappini C., 2013, Astron. Nachr., 334, 595

Conroy C., 2012, ApJ, 758, 21

Crawford J. A., 1953, PASP, 65, 210

Cunha K. et al., 2015, ApJ, 798, L41

D'Ercole A., Vesperini E., D'Antona F., McMillan S. L. W., Recchi S., 2008, MNRAS, 391, 825

D'Orazi V., Gratton R., Lucatello S., Carretta E., Bragaglia A., Marino A. F., 2010, ApJ, 719, L213

de Jager C., Nieuwenhuijzen H., van der Hucht K. A., 1988, A&AS, 72, 259

Dotter A., Chaboyer B., Jevremović D., Kostov V., Baron E., Ferguson J. W., 2008, ApJS, 178, 89

Faber S. M., 1983, in West R. M.,ed., Proc. IAU Symp. 6, Highlights of Astronomy, Kluwer, Dordrecht,p. 165

Fall S. M., Zhang Q., 2001, ApJ, 561, 751

Federrath C., Schrön M., Banerjee R., Klessen R. S., 2014, ApJ, 790, 128

Finkelstein S. L., 2016, PASA, 33, e037

Fioc M., Rocca-Volmerange B., 1999, preprint (ArXiv Astrophysics e-prints)

Girardi L., Costa G., Chen Y., Goudfrooij P., Bressan A., Marigo P., Bellini A., 2019, MNRAS, 488, 696

Goudfrooij P., 2018, ApJ, 857, 16

Goudfrooij P., Girardi L., Bellini A., Bressan A., Correnti M., Costa G., 2018, ApJ, 864, L3

Greggio L., Renzini A., 1990, ApJ, 364, 35

Grevesse N., Noels A., 1993, in Prantzos N., Vangioni-Flam E., Casse M., eds, Origin and Evolution of the Elements, Cambridge University Press, Cambridge, p. 15

Hennebelle P., Chabrier G., 2009, ApJ, 702, 1428

Herwig F., VandenBerg D. A., Navarro J. F., Ferguson J., Paxton B., 2012, ApJ, 757, 132

Hopkins P. F., 2012, MNRAS, 423, 2037

Johnson C. I., Caldwell N., Rich R. M., Walker M. G., 2017a, AJ, 154, 155

Johnson C. I., Caldwell N., Rich R. M., Mateo M., Bailey III J. I., Clarkson W. I., Olszewski E. W., Walker M. G., 2017b, ApJ, 836, 168

Karakas A. I., 2014, MNRAS, 445, 347

Karakas A. I., Shingles L. J., 2017, Mem. Soc. Astron. Italiana, 88, 244

Karakas A. I., Marino A. F., Nataf D. M., 2014, ApJ, 784, 32

Kippenhahn R., Weigert A., 1990, Astronomy and Astrophysics Library, Stellar Structure and Evolution, XVI, Springer-Verlag, Berlin, Heidelberg, New York, p. 468

Kruijssen J. M. D., Portegies Zwart S. F., 2009, ApJ, 698, L158

Kruijssen J. M. D., Pfeffer J. L., Crain R. A., Bastian N., 2019a, MNRAS, 486, 3134

Kruijssen J. M. D., Pfeffer J. L., Reina-Campos M., Crain R. A., Bastian N., 2019b, MNRAS, 486, 3180

Krumholz M. R., Federrath C., 2019, Front. Astron. Space Sci., 6, 7

Kurucz R. L., 1970, SAO Special Report, 309

Kurucz R., 1993, SYNTHE Spectrum Synthesis Programs and Line Data. Kurucz CD-ROM No. 18, Smithsonian Astrophysical Observatory, Cambridge, MA

Kurucz R. L., 2005, Memorie della Societa Astronomica Italiana Supplementi, 8, 14

Kurucz R. L., 2013, ATLAS12: Opacity sampling model atmosphere program, Astrophysics Source Code Library. record ascl:1303.024

Kurucz R. L., Avrett E. H., 1981, SAO Special Report, 391

Lagioia E. P. et al., 2018, MNRAS, 475, 4088

Lagioia E. P., Milone A. P., Marino A. F., Dotter A., 2019, ApJ, 871, 140

Lamers H. J. G. L. M., Baumgardt H., Gieles M., 2013, MNRAS, 433, 1378

Lee Y.-W., Demarque P., Zinn R., 1994, ApJ, 423, 248

Li C., Sun W., de Grijs R., Deng L., Wang K., Cordoni G., Milone A. P., 2019, ApJ, 876, 65

Lucatello S., Sollima A., Gratton R., Vesperini E., D'Orazi V., Carretta E., Bragaglia A., 2015, A&A, 584, A52

MacLean B. T., Campbell S. W., De Silva G. M., Lattanzio J., D'Orazi V., Simpson J. D., Momany Y., 2016, MNRAS, 460, L69

Mandelker N., van Dokkum P. G., Brodie J. P., van den Bosch F. C., Ceverino D., 2018, ApJ, 861, 148

Marín-Franch A., Cassisi S., Aparicio A., Pietrinferni A., 2010, ApJ, 714, 1072

Marino A. F., Przybilla N., Milone A. P., Da Costa G., D'Antona F., Dotter A., Dupree A., 2018, AJ, 156, 116

Martell S. L., Grebel E. K., 2010, A&A, 519, A14

Martocchia S. et al., 2017, MNRAS, 468, 3150

Milone A. P. et al., 2017, MNRAS, 464, 3636

Muratov A. L., Gnedin O. Y., 2010, ApJ, 718, 1266

Nataf D. M. et al., 2019, AJ, 158, 14

Nataf D. M., 2014, MNRAS, 445, 3839

Nataf D. M., Gould A., Pinsonneault M. H., Stetson P. B., 2011, ApJ, 736, 94

Nataf D. M., Gould A., Pinsonneault M. H., 2012, AcA, 62, 33

Norris J. E., 2004, ApJ, 612, L25

Norris J., Cottrell P. L., Freeman K. C., Da Costa G. S., 1981, ApJ, 244, 205

Nugis T., Lamers H. J. G. L. M., 2000, A&A, 360, 227

Paardekooper J.-P., Khochfar S., Dalla Vecchia C., 2015, MNRAS, 451, 2544

Padoan P., Nordlund Å., 2002, ApJ, 576, 870

Pietrinferni A., Cassisi S., Bono G., Stetson P. B., Iannicola G., Castellani V., Buonanno R., Zoccali M., 2006a, Mem. Soc. Astron. Italiana, 77, 144

Pietrinferni A., Cassisi S., Salaris M., Castelli F., 2006b, ApJ, 642, 797

Pietrinferni A., Cassisi S., Salaris M., Percival S., Ferguson J. W., 2009, ApJ, 697, 275

Piotto G. et al., 2007, ApJ, 661, L53

Pozzetti L., Maraston C., Renzini A., 2019, MNRAS, 485, 5861

Renzini A., 2013, Mem. Soc. Astron. Italiana, 84, 162

Renzini A., 2017, MNRAS, 469, L63

Ricotti M., 2002, MNRAS, 336, L33

Ricotti M., 2004, in Lamers H. J. G. L. M., Smith L. J., Nota A., eds, ASP Conf. Ser Vol. 322, The Formation and Evolution of Massive Young Star Clusters, Astron. Soc. Pac., San Francisco, p. 509

Roy A., Sutherland R. S., Krumholz M. R., Heger A., Dopita M. A., 2019, MNRAS, 498, 3861

Salaris M., Cassisi S., 2005, Evolution of Stars and Stellar Populations, Wiley-VCH, pp. 400

Salpeter E. E., 1952, ApJ, 115, 326

Salpeter E. E., 1955, ApJ, 121, 161

Sandage A., Wildey R., 1967, ApJ, 150, 469

Schiavon R. P. et al., 2017, MNRAS, 465, 501

Shingles L. J., Doherty C. L., Karakas A. I., Stancliffe R. J., Lattanzio J. C., Lugaro M., 2015, MNRAS, 452, 2804

Sollima A., Baumgardt H., 2017, MNRAS, 471, 3668

Spitzer L., 1987, Dynamical evolution of globular clusters, Princeton Univ. Press, Princeton, NJ

Tang J., Bressan A., Rosenfield P., Slemer A., Marigo P., Girardi L., Bianchi L., 2014, MNRAS, 445, 4287

Ting Y.-S., Conroy C., Goodman A., 2015, ApJ, 807, 104

Valcarce A. A. R., Catelan M., 2011, A&A, 533, A120

van den Bergh S., 1967, AJ, 72, 70

Vanzella E. et al., 2019a, MNRAS, 491, 1093

Vanzella E. et al., 2019b, MNRAS, 483, 3618

Vink J. S., de Koter A., Lamers H. J. G. L. M., 2000, A&A, 362, 295

Vink J. S., de Koter A., Lamers H. J. G. L. M., 2001, A&A, 369, 574

Webb J. J., Leigh N. W. C., 2015, MNRAS, 453, 3278

Wilson C. D., Harris W. E., Longden R., Scoville N. Z., 2006, ApJ, 641, 763

Wright E. L., 2006, PASP, 118, 1711

Zepf S. E., Ashman K. M., 1993, MNRAS, 264, 611

Zick T. O., Weisz D. R., Boylan-Kolchin M., 2018, MNRAS, 477, 480

SUPPORTING INFORMATION

Supplementary data are available at *MNRAS* online.

Table 1. A subsample of predicted magnitude differences between a helium-enriched ($Y = 0.40$) and helium-normal population ($Y = 0.28$).

Please note: Oxford University Press is not responsible for the content or functionality of any supporting materials supplied by the authors. Any queries (other than missing material) should be directed to the corresponding author for the article.

This paper has been typeset from a T$_{\rm E}$X/L$^{\rm A}$T$_{\rm E}$X file prepared by the author.